Cerebral Cortex, March 2019;29: 1150–1161

doi: 10.1093/cercor/bhy021
Advance Access Publication Date: 7 February 2018
Original Article

ORIGINAL ARTICLE

Determinants of Optogenetic Cortical Spreading Depolarizations

David Y. Chung[1,2], Homa Sadeghian[1], Tao Qin[1], Sevda Lule[3], Hang Lee[4], Fahri Karakaya[5], Stacy Goins[6], Fumiaki Oka[1,7], Mohammad A. Yaseen[8], Thijs Houben[9], Else A. Tolner[9], Arn M. J. M. van den Maagdenberg[9], Michael J. Whalen[3], Sava Sakadžić[8] and Cenk Ayata[1,2]

[1]Department of Radiology, Massachusetts General Hospital, Charlestown, MA, USA, [2]Department of Neurology, Massachusetts General Hospital, Boston, MA, USA, [3]Department of Pediatrics, Massachusetts General Hospital, Boston, MA, USA, [4]Department of Medicine, Massachusetts General Hospital, Boston, MA, USA, [5]University of Massachusetts Dartmouth, Dartmouth, MA, USA, [6]Program in Molecular Biology and Biochemistry, Middlebury College, Middlebury, VT, USA, [7]Department of Neurosurgery, Yamaguchi University School of Medicine, Ube, Japan, [8]Department of Radiology, Athinoula A. Martinos Center for Biomedical Imaging, Massachusetts General Hospital, Charlestown, MA, USA and [9]Departments of Neurology and Human Genetics, Leiden University Medical Center, Leiden, The Netherlands

Address correspondence to David Y. Chung and Cenk Ayata, Massachusetts General Hospital, 149 13th Street, Charlestown, MA 02129, USA. Email: dychung@mgh.harvard.edu (David Y. Chung); cayata@mgh.harvard.edu (Cenk Ayata).

Abstract

Cortical spreading depolarization (SD) is the electrophysiological event underlying migraine aura, and a critical contributor to secondary damage after brain injury. Experimental models of SD have been used for decades in migraine and brain injury research; however, they are highly invasive and often cause primary tissue injury, diminishing their translational value. Here we present a non-invasive method to trigger SDs using light-induced depolarization in transgenic mice expressing channelrhodopsin-2 in neurons (Thy1-ChR2-YFP). Focal illumination (470 nm, 1–10 mW) through intact skull using an optical fiber evokes power-dependent steady extracellular potential shifts and local elevations of extracellular [K^+] that culminate in an SD when power exceeds a threshold. Using the model, we show that homozygous mice are significantly more susceptible to SD (i.e., lower light thresholds) than heterozygous ChR2 mice. Moreover, we show SD susceptibility differs significantly among cortical divisions (motor, whisker barrel, sensory, visual, in decreasing order of susceptibility), which correlates with relative channelrhodopsin-2 expression. Furthermore, the NMDA receptor antagonist MK-801 blocks the transition to SD without diminishing extracellular potential shifts. Altogether, our data show that the optogenetic SD model is highly suitable for examining physiological or pharmacological modulation of SD in acute and longitudinal studies.

Key words: cortical spreading depression, electrophysiology, mouse, optogenetics, potassium

Introduction

Spreading depression (a.k.a. spreading depolarization, SD) is a massive neuronal and glial depolarization wave that slowly propagates in gray matter (Leão 1944; Ayata and Lauritzen 2015). SD is the likely electrophysiological correlate of migraine aura, induces neuroinflammation, and triggers headache

(Ayata 2010; Eikermann-Haerter et al. 2012). Moreover, recurrent SD waves develop in injured brain and worsen outcome (Dreier et al. 2006, 2009; Fabricius et al. 2008; Bosche et al. 2010; Dreier 2011; Chung et al. 2016; Hartings et al. 2016; Oka et al. 2016). Therefore, experimental models of SD are increasingly used to examine the pathogenesis and develop novel therapeutics (Ayata 2009). However, existing models rely upon direct chemical, electrical, or mechanical perturbation of the cerebral cortex through a craniotomy, which cause direct injury at the stimulation site as a potential confounder (Ayata 2013). Moreover, cumulative injury precludes reliable induction of SDs repeatedly in the same animal over days or months, or in unanesthetized animals, altogether diminishing the translational value of such models.

Recently, optogenetics was employed to trigger cortical SDs using light (Houben et al. 2016). Optogenetic SDs were electrophysiologically and hemodynamically identical to SDs induced by conventional means. Here, we present a comprehensive characterization of optogenetic SDs in 2 strains of transgenic mice expressing channelrhodopsin-2 in neurons (Thy1-ChR2-YFP). We examined the relationship between the light intensity and the electrophysiological and extracellular $[K^+]$ changes at the stimulated focus, defined the threshold intensity that triggers an SD in 4 different brain regions, described its modulation by stimulus duration, age and sex, and showed that optogenetic SDs are NMDA receptor-dependent. Moreover, we describe potential confounders and pitfalls of the model. Altogether, this noninvasive optogenetic SD model may enhance the translational value of future studies.

Materials and Methods

All experimental procedures were carried out in accordance with the Guide for Care and Use of Laboratory Animals (NIH Publication No. 85-23, 1996), and the ARRIVE guidelines, with the exception of random allocation and blinding because all testing involved natural variables (e.g., transgenic $ChR2^{+/+}$ vs. $ChR2^{+/-}$, male vs. female). All protocols were approved by the institutional review board (MGH Subcommittee on Research Animal Care). We used Thy1-ChR2-YFP mice (B6.Cg-Tg(Thy1-COP4/EYFP)9Gfng/J [heterozygous line 9; $ChR2^{+/-}$] and B6.Cg-Tg (Thy1-COP4/EYFP)18Gfng/J [homozygous line 18; $ChR2^{+/+}$]; Jackson Laboratories, Bar Harbor, ME, USA) in all experiments (Wang et al. 2007). In a subset of experiments we used wild-type mice ($ChR2^{-/-}$; littermates of $ChR2^{+/-}$ or C57BL/6J from Charles River Laboratories, Wilmington, MA, USA). All mice (male or female) were studied between 12 and 54 weeks of age (22.0 ± 2.8 g). Arterial pH, pO_2, pCO_2, and blood pressure were monitored via a femoral artery catheter and maintained within normal limits (BP = 89 ± 12 mmHg, pH = 7.36 ± 0.06, pCO_2 = 37 ± 8 mmHg, pO_2 = 115 ± 14 mmHg). Rectal temperature was kept at 37 °C using a thermostatic heating pad. Technical failure was the only exclusion criterion. One animal was excluded due to arterial line malfunction and one animal was excluded due to subdural hematoma formation during drilling of a burr hole. Mice were anesthetized with isoflurane (5% induction, 1% maintenance, in 70% N_2/30% O_2) and allowed to breathe spontaneously. The head was fixed in a stereotaxic frame. To augment analgesia we applied 2% xylocaine paste around skin incisions, and to protect the eyes we applied lubricating ointment. In survival experiments (n = 8), we closely monitored the animals for 24 h following the procedure and recovery from anesthesia to ensure for signs of pain and discomfort, and did not observe any.

Optogenetic Stimulation

After a midline scalp incision and reflection, the skull was cleared of connective tissue and covered with mineral oil to prevent drying. The optic fiber was placed perpendicular to the skull surface, and a layer of mineral oil was maintained between the probe tip and the skull at all times for consistent optical coupling. Optogenetic stimulation light was provided through a 400-μm diameter fiber by a 470 nm LED (LED: MF470F3; LED driver: DC2100; Thorlabs, Newton, NJ, USA) controlled by the computer and analog-digital converter (PowerLab, ADInstruments, Colorado Springs, CO, USA). Light intensity was adjusted to deliver 1–10 mW at the skull surface. Delivered power was calibrated off line using a power meter (PM16-130, Thorlabs). Using this set up, escalating light power in 1-mW steps between 1 and 10 mW was applied for 2, 5, 10 or 20 s in different experimental sessions to examine the extracellular potential shifts directly induced by light stimulation. SD threshold was determined in each hemisphere at the following coordinates relative to bregma: 1) 2 mm anterior and 2 mm lateral (motor), 2) 1 mm posterior and 3 mm lateral (whisker barrel), 3) 1 mm posterior and 2 mm lateral (somatosensory shoulder region), and 4) 3.5 mm posterior and 2.5 mm lateral (visual) according to the Paxinos and Franklin mouse brain atlas (Paxinos and Franklin 2001).

Determination of Electrical and KCl Concentration Thresholds of SD

In $ChR2^{-/-}$ mice, we determined the SD susceptibility in visual and motor cortices as described in detail previously (Ayata et al. 2006; Eikermann-Haerter et al. 2011; Ayata 2013). To determine thresholds for KCl- and bipolar electrode-induced SDs, 2 burr holes with a diameter of 2 mm were drilled at (from bregma): 1) 3.5 mm posterior, 2.5 mm lateral (occipital) and 2) 2.0 mm anterior, 2.0 mm lateral (frontal). Cotton balls (1.5 mm diameter) soaked with stepwise increasing KCl solutions of 10, 20, 40, 60, 80, 100, and 120 mM, made isotonic by NaCl, were placed on the pial surface for 3 min. If no SD was elicited at a given concentration, the cotton ball was removed and the cortical surface was washed with normal saline. After 2 min another cotton ball with the next higher KCl concentration was placed. Electrical SD threshold was determined by escalating cathodal square pulses (0.5–1024 μC; 0.2 mA for 2.5, 5, 10, 20, 40, 80, 160, 320, and 640 ms, followed by 0.4 mA for 640 ms, 0.8 mA for 640 ms, and 1.6 mA for 640 ms) delivered via a bipolar electrode on the pial surface. A resting period of 3 min was used to determine whether an SD was evoked prior to moving to the next higher stimulus level.

Monitoring of SD

We monitored SD occurrence using different modalities in different experimental paradigms. In most experiments, we employed reflectance (i.e., optical intrinsic signal) imaging to detect SD occurrence by using the attendant cerebral blood volume changes as a surrogate. In a subset of experiments, we confirmed these electrophysiologically by recording extracellular potential shifts using an intracortical glass micropipette placed directly under the optic fiber inserted at 40° from vertical, and advanced 500 μm, corresponding to an approximate cortical depth of 380 μm. In a smaller number of experiments, we additionally used laser speckle or Doppler flowmetry to monitor cortical perfusion changes, which are highly sensitive

and specific as a surrogate to detect SD (Ayata 2013; von Bornstadt et al. 2015). To determine the amplitude, duration, and propagation speed of SDs in $ChR2^{+/+}$ and $ChR2^{-/-}$ mice, 2 glass microelectrodes were placed 2 mm apart, away from the SD induction site. In $ChR2^{+/+}$ mice, a suprathreshold light pulse of 3 mW was applied over motor cortex (2 mm anterior and 2 mm lateral to bregma), followed 15 min later by 1 M KCl applied to the same position through a burr hole. In $ChR2^{-/-}$ mice, only the 1 M KCl application was performed.

ChR2 and NeuN Expression

Thy1-ChR2-$YFP^{+/-}$ mice were perfused with 4% PFA, the brains were harvested, and post-fixed in 4% PFA for 24 h. Brains were then cryoprotected in 30% sucrose for 48 h and snap frozen in 2-methylbutane cooled to −40 °C. Brains were then embedded in M-1 Embedding Matrix (Thermo Fisher Scientific, Waltham, MA, USA) and cut into 30-μm thick sagittal sections using a cryostat and floated in phosphate-buffered saline with sodium azide. Tissue sections were washed 3 times in 1× PBS, blocked with 5% donkey normal serum in 1× PBS, and incubated in antibody solution containing 3% donkey normal serum and Monoclonal Anti-NeuN antibody (1:300 dilution, Millipore Chemicon, Billerica, MA, USA) overnight at 4 °C. Tissue sections were then washed 3 times in 1× PBS and incubated with antibody solution containing 3% normal donkey serum, FITC-conjugated anti-GFP antibody (1:300 dilution, Abcam, Cambridge, MA, USA) and Cy3-conjugated donkey anti-mouse IgG antibody (1:300 dilution, Jackson ImmunoResearch, West Grove, PA, USA) for 1 h at room temperature. Sections were washed 3 times with 1× PBS, mounted onto ionized glass slides (Thermo Fisher Scientific), and cover-slipped with Fluoro-gel Mounting Medium (Electron Microscopy Services, Hatfield, PA, USA). Immunofluorescence was visualized using a Nikon T3000 fluorescence microscope and QImaging Retiga-2000 R-F-M digital camera running Nikon NIS Elements BR software (Melville, NY, USA). Images were stitched and quantified using ImageJ.

Extracellular [K^+] Measurements

K^+-sensitive electrodes were prepared as previously described with some modifications (Ballanyi et al. 1987). Borosilicate capillaries were pulled with a p80/PC brown flaming micropipette puller (Sutter Instruments, Novato, CA, USA). The ion-sensitive barrel was back-filled with potassium chloride (100 mM, in 154 mM NaCl) and the tip (2–3 μM) was silanized and filled with a K^+-sensitive resin (Liquid Ion Exchanger IE190, WPI, Sarasota FL, USA). The reference barrel was filled with sodium chloride (154 mM, 10 MΩ). An Ag/AgCl reference electrode was placed subcutaneously in the neck. For optogenetic light stimulation experiments, the potassium-selective electrode was angled through a burr hole to position the tip of the electrode underneath the optical light fiber (whisker barrel cortex, 1 mm posterior and 3 mm lateral to bregma).

MK-801 Treatment

To test the NMDA receptor dependence of optogenetic SDs, MK-801 (#M107; Sigma-Aldrich, St. Louis, MO, USA) was injected intraperitoneally at a dose of 1 mg/kg 30 min prior to SD threshold determination. If 1 mg/kg failed to block an SD, an additional 1 mg/kg was given and threshold determination was repeated.

Skull Thickness and Transmittance Experiments

Skulls were removed, preserved in mineral oil, and immobilized between 2 glass coverslips. The optical fiber was positioned over the skull between the coverslips, and light transmittance was determined using a light power meter (PM16-130, Thorlabs).

Chronic Cranial Preparation for Longitudinal SD Induction

Chronic intact skull windows were prepared as previously described (Silasi et al. 2016). Briefly, the surface of the skull was exposed and the overlying periosteum was removed. A circular glass coverslip was cut to the size of the cranial window. C&B Metabond cement was prepared using Clear L-Powder (Parkell, Edgewood, NY, USA) and applied to the surface of the dried skull. The cut coverslip was placed on the prepared skull and additional cement was added to fill in gaps between the coverslip and skull.

Cortical Temperature Experiments

To determine the change in brain temperature in response to light stimulation, we inserted a BAT-12/IT-23 thermocouple microprobe thermometer (Physitemp, Clifton, NJ, USA) through a burr hole such that the tip of the thermometer was immediately under the light source. We applied a light stimulation protocol of 60 s on, 60 s off, in powers ranging from 1 to 10 mW while recording changes in temperature in wild-type C57BL/6 J and Thy1-ChR2-YFP mice.

Histological Assessment of Injury

To determine whether the light intensities used in this study cause direct tissue injury, we applied 10 mW of light to motor cortex for 20 s (i.e., highest intensity and duration combination), and sacrificed the mice 24 h later and performed Fluoro-Jade C staining. Brains were perfused and fixed in PFA. Tissue sections were mounted and air-dried onto ionized glass slides. Sections were immersed in basic ethanol solution for 5 min, briefly washed with 70% ethanol followed by distilled water, and incubated in 0.06% potassium permanganate solution for 10 min. Sections were washed briefly in distilled water and incubated in FluoroJade C solution containing 0.1% acetic acid and 0.0002% FluoroJade C (AAT Bioquest, Sunnyvale, CA, USA) for 15 min. Tissue sections were rinsed 3 times in distilled water, dehydrated in butanol, and cover-slipped with DPX mounting medium (Sigma, St Louis, MO, USA). Fluorescence was visualized as above.

Statistics

We applied general linear random intercept mixed effects modeling to build a multivariable linear prediction model of mean threshold power with sex, age, zygosity, region of stimulation, pH, pCO_2, pO_2, mean arterial blood pressure, hemisphere (left or right), time elapsed since the beginning of anesthesia, stimulus duration, light intensity and order of SD induction. This method was applied in order to take into account the correlated repeated measures on multiple regions within each experimental mouse. In addition, we used paired samples *t*-test and Pearson's linear correlation (*r*) as appropriate for different datasets, as reported in the figures. All tests were 2-tailed. $P < 0.05$ was considered statistically significant.

Results

Light application through the intact skull for 10 or 20 s consistently induced a single SD in ChR2 transgenic mice, as detected by optical intrinsic signal imaging (Supplemental Video), extracellular recordings using an intracortical glass micropipette under the optical fiber (Fig. 1A,B), or by laser Doppler (Fig. 1C,D) or speckle flowmetry (not shown). In contrast, the same illumination never induced an SD in non-transgenic (wild-type) $ChR2^{-/-}$ mice ($n = 6$ mice) even at the longest durations (20 s) and highest stimulation intensities (10 mW) tested (data not shown). The electrophysiological features of optogenetic and KCl-induced SDs in $ChR2^{+/+}$ mice (i.e., propagation speed, amplitude, duration) (Table 1) were within previously reported normal ranges for KCl-induced SDs in wild-type mice (Eikermann-Haerter et al. 2015). Notably, light intensities of up to 10 mW for 20 s did not cause cell death or injury, examined by FluoroJade C staining 24 h later ($n = 3$ $ChR2^{+/-}$ and $ChR2^{-/-}$ each; data not shown), consistent with prior reports of the threshold stimulation for neurotoxic effects (Anikeeva et al. 2011).

We next applied stepwise escalating intensities of light (1–10 mW) for 10 or 20 s every 2 min to determine the threshold light intensity to trigger an SD in 4 different cortical regions (motor, whisker barrel, somatosensory, visual), in male and female $ChR2^{+/-}$ and $ChR2^{+/+}$ mice of various ages ($n = 44$; Fig. 2). We then used a multivariable linear prediction model to isolate the independent predictors of optogenetic SD susceptibility in the pooled dataset ($n = 30$ after excluding mice with missing data; see Supplemental Data for the raw dataset). Our analysis revealed marked regional differences in susceptibility to light-induced SD ($P < 0.0001$). Motor and whisker barrel cortices consistently showed lower thresholds (i.e., higher susceptibility) than the rest of the primary somatosensory cortex (see Supplemental Table for individual comparisons). In contrast, visual cortex was quite resistant requiring very high light intensities, and often failed to develop an SD even at the highest intensity (10 mW) delivered for 20 s. This regional propensity was evident in both $ChR2^{+/-}$ and $ChR2^{+/+}$. As anticipated, $ChR2^{+/+}$ mice were more susceptible to optogenetic SD than $ChR2^{+/-}$ ($P < 0.0001$), and 20-s stimulation yielded lower intensity thresholds than 10-s stimulation ($P < 0.0001$). Notably, female SD thresholds were slightly lower (by 0.7 mW; $P = 0.04$) than male thresholds. In contrast, the model did not support age as a statistically or biologically significant independent predictor (estimated 0.01 mW per week of age; $P = 0.27$).

As expected, the threshold did not differ between right versus left hemisphere ($P = 0.47$). The number of SDs triggered in the same hemisphere prior to each threshold testing also influenced the threshold in the pooled cohort (estimated 0.5 mW increase for every SD; $P = 0.026$; see Supplemental Table for individual comparisons). We also found a significant direct relationship between the anesthesia duration and the threshold (estimated 0.8 mW increase for every hour; $P = 0.0012$). Lastly, we did not see an effect of arterial blood pressure, pH, pCO_2 or pO_2 ($P = 0.79$, 0.96, 0.50, 0.72, respectively) within the physiological ranges maintained in this study.

The magnitude of regional differences in optogenetic SD thresholds was rather large. Because regional differences in SD susceptibility have been suggested in the past (Bogdanov et al. 2016), we next determined the electrical stimulation intensity and KCl concentration thresholds for SD induction in the visual and motor cortices (Fig. 3). These more conventional methods showed a trend in the opposite direction, where visual cortex tended to be more susceptible than motor cortex when measured in the same animal. These data suggested that the regional differences in optogenetic SD susceptibility did not reflect innate SD susceptibility of these cortical regions.

To explain the incongruence, we examined the regional expression of ChR2 using epifluorescence microscopy on sagittal tissue sections from $ChR2^{+/-}$. We found marked differences in ChR2 expression among the 4 cortical regions (Fig. 4A), which

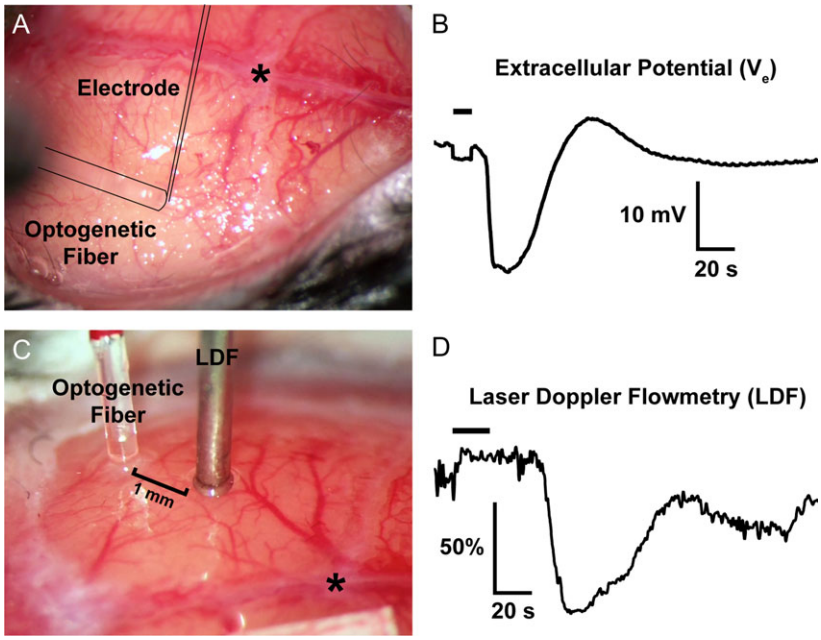

Figure 1. Representative optogenetic SDs through the intact skull. (A,B) The optical fiber, out of focus in this image, is outlined, as is the glass micropipette inserted through a <100-μm burr hole next to the optical fiber to record the extracellular slow potential shifts (V_e) in the right whisker barrel cortex. (C,D) A laser Doppler probe (LDF) away from the optical fiber non-invasively detects the propagating blood flow changes associated with an SD that was optogenetically induced in left visual cortex. SD induction and subsequent propagating blood flow changes are also shown in the Supplemental Video at 20x speed. Horizontal bars on the tracings show illumination period. *, bregma.

corresponded well with the susceptibility to light-induced SDs in these regions. There was a significant inverse relationship between the SD threshold and ChR2 expression (Fig. 4B). Interestingly, the inverse relationship between SD threshold and ChR2 expression was stronger for upper cortical layers, and did not reach statistical significance for depths below 500 μm. This was consistent with the fact that 470 nm optogenetic stimulation light has a shallow penetration depth with more than 90% attenuation within 250 μm (Uhlirova et al. 2016). Because we induced optogenetic SDs through the intact skull, regional differences in skull thickness (Fig. 4C,D) could affect light transmittance and influence the apparent SD thresholds. We, therefore, measured the light transmittance of skull overlying the motor, whisker barrel, somatosensory and visual cortices, and did not find a significant difference (Fig. 4E,F).

We reasoned that regions with higher ChR2 expression might develop larger light-induced depolarizations to explain the lower SD thresholds. Direct microelectrode recordings from the illuminated cortex under the optic fiber revealed negative extracellular potential shifts with fast on/off and superimposed

Table 1 Amplitude, duration, and propagation speed of optogenetic or KCl-induced SDs in $ChR2^{+/+}$ and $ChR2^{-/-}$ mice

	$ChR2^{-/-}$ ($n = 7$)	$ChR2^{+/+}$ ($n = 4$)	
	KCl-induced SD	KCl-induced SD	Optogenetic SD
Amplitude (mV)	24.7 ± 1.0	19.8 ± 2.1*	21.8 ± 2.6
Duration (s)	34 ± 4	37 ± 14	37 ± 11
Speed (mm/min)	3.0 ± 0.2	3.0 ± 0.2	3.0 ± 0.3

Data are mean ± standard deviation. *$P < 0.05$ vs. KCl-induced SDs in $ChR2^{-/-}$; 1-way ANOVA followed by Tukey's multiple comparisons test.

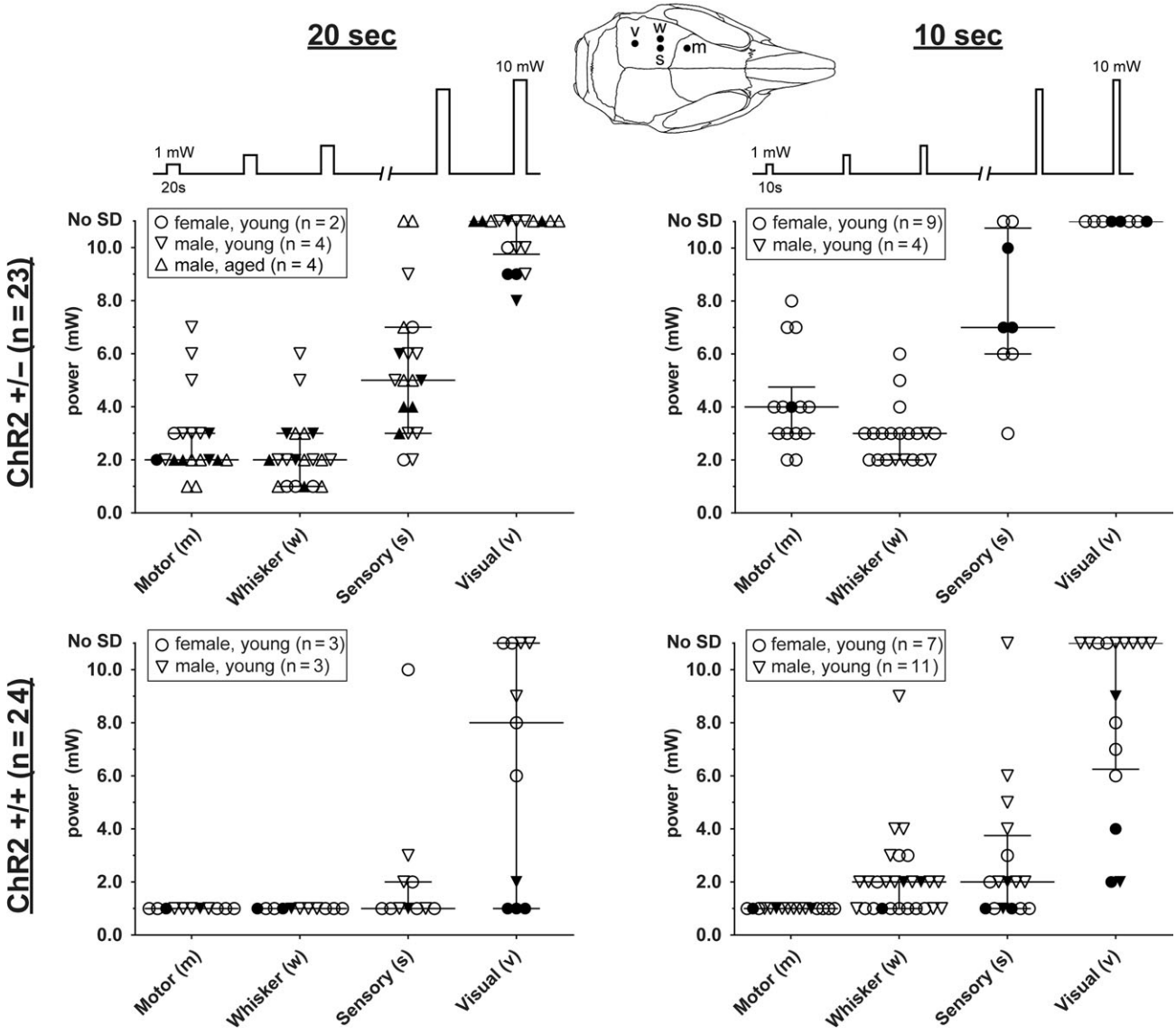

Figure 2. Optogenetic SD thresholds. The threshold light intensities that triggered an SD are shown for $ChR2^{+/-}$ (upper) and $ChR2^{+/+}$ (lower) mice using 10- (right) or 20-s (left) stimulation paradigms. Each SD threshold determination involved stepwise escalation of light intensity as shown on top. Inset shows stimulation regions. Sample sizes indicate the number of mice. Each animal had multiple SD threshold trials. Each data point represents the threshold in 1 trial. Failure of SD induction despite maximum stimulus is also indicated (No SD). Filled symbols indicate the results of the first SD threshold trial in a hemisphere, whereas open symbols indicate subsequent trials. Median and interquartile ranges are also shown. Young mice were 12–18 weeks and aged mice were ~1 year old.

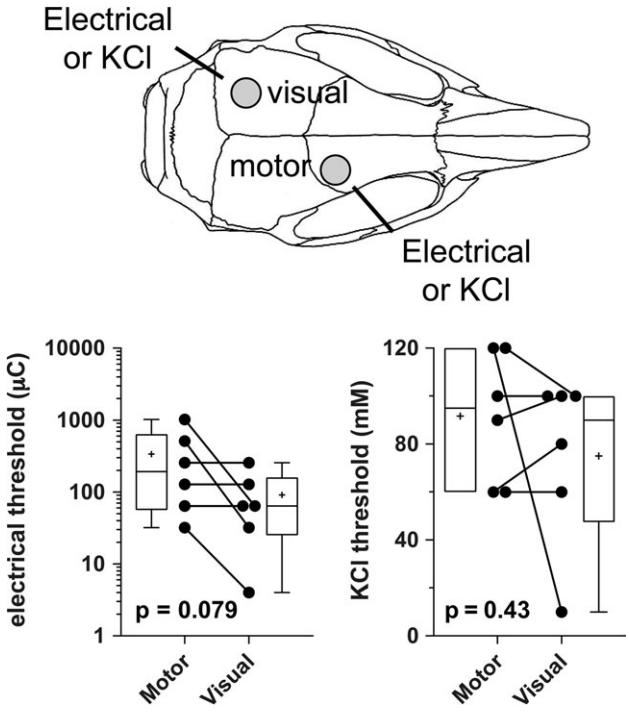

Figure 3. Thresholds for electrical and KCl stimulation-induced SDs in motor and visual cortices. Cartoon shows the electrical stimulation and KCl application sites for threshold determination. Whisker-box plots show the interquartile and full ranges for electrical (log) and KCl concentration thresholds for SD induction (horizontal line, median; +, mean), analyzed using paired *t*-test (2 tailed; $n = 6$ mice). Individual data points are also shown.

slow on/off components (Fig. 5*A*). Such potential shifts never occurred in wild-type ($ChR2^{-/-}$) mice (Fig. 5*B*). The power-dependence of the fast component approached near maximal at the highest power tested and likely represented currents evoked directly by ChR2 activation (Fig. 5*C*). The amplitude of fast "on" negative potential shift was larger than the amplitude of fast "off" shift possibly due to partial inactivation during illumination. In contrast, the slow component tended to increase over time, suggesting recruitment of other currents by the ChR2-driven fast depolarization. Both the fast and slow components were significantly larger in whisker barrel cortex compared with visual cortex, consistent with higher relative ChR2 expression and lower SD thresholds. The whisker/visual cortex negative potential shift ratio was remarkably constant within each animal (1.6 and 2.7 for the fast and slow components, respectively; Fig. 5*D*,*E*).

Since the extracellular K^+ concentration ($[K^+]_e$) may be a critical determinant for SD induction, we measured $[K^+]_e$ during optogenetic activation. The extracellular negative potential shifts during illumination in the whisker barrel cortex were always associated with $[K^+]_e$ elevations, the amplitude of which were directly related to light power (Fig. 5*F*,*G*). At suprathreshold stimulations, light-induced $[K^+]_e$ rise culminated in an SD with associated massive $[K^+]_e$ surge (Fig. 5*H*). The amplitude and duration of the optogenetically induced $[K^+]_e$ surge did not differ from that induced by topical KCl (Table 2). Due to the slow response time and the lack of precision in electrode calibration, however, we refrained from calculating the local $[K^+]_e$ during stimulation in this study.

We next examined how light-induced negative potential shifts transitioned into an SD in the whisker barrel cortex. Using cortical microelectrodes placed immediately under the optic fiber, we found that most SDs started with a delay of 10 s or more after the end of the illumination and the associated negative potential shift (Fig. 6). Surprisingly, this delay was independent of the stimulation power or the potential shift amplitude, and even longer in $ChR2^{+/+}$ mice compared with $ChR2^{+/-}$ mice. As a potential explanation for the delay in SD onset at the recording site, the origin of SDs might be farther away from the recording electrode under the optic fiber light source. Because SD propagates at a speed of ~3 mm/min (~50 μm/s), a latency of more than 10 s implicated an SD origin more than 0.5 mm away from the recording site at the center of illumination. However, given the limited tissue penetration of 470 nm stimulation light (99% attenuation within 0.5 mm) (Uhlirova et al. 2016), it is unlikely that SDs originated this far from the center of illumination. We confirmed this in our optical intrinsic signal images, which showed that SDs always originated from directly under the optic fiber light source (Supplemental Video).

As an alternative explanation for the delay in SD onset, optogenetic stimulation might initiate yet unknown neuronal or glial processes that do not by themselves cause extracellular potential shifts, but over time lead to the initiation of an SD. Activation of *N*-methyl-D-aspartate (NMDA) subtype glutamate receptors is critical for SD initiation and propagation in normal brain. To test the contribution of NMDA receptors to optogenetically induced extracellular potential shifts and SD initiation, we treated the animals with MK-801 (1 or 2 mg/kg). MK-801 blocked the development of local SD-like depolarizations and initiation of a propagating SD, but surprisingly did not diminish either the fast or the slow component of the extracellular negative potential shift under the optic fiber during light stimulation in the same animal. Instead, prevention of transition to SD by MK-801 unmasked a slow afterpotential that emerged and peaked ~5 s after the end of illumination, and lasted up to 20 s. Although these afterpotentials could be as high as 8 mV, they never culminated in an SD after treatment with MK-801 (Fig. 7*D*).

To employ optogenetics for chronic daily non-invasive SD induction (Houben et al. 2016), we adapted an intact skull preparation using translucent cement and a glass coverslip. Optogenetic illumination of the motor cortex through the cement and coverslip using the lowest stimulus intensity (1 mW for 10 s) in $ChR2^{+/+}$ mice reliably induced an SD, detected using optical intrinsic signal (Fig. 8) and laser speckle contrast imaging (not shown). Optogenetic SDs could be induced in the same $ChR2^{+/+}$ animal at the same light intensity daily for at least 4 days ($n = 8$).

Finally, we examined whether illumination causes tissue heating by measuring brain temperature directly under the optic fiber during escalating light intensities (1–10 mW, 60 s) using a microthermometer in $ChR2^{+/-}$ and $ChR2^{-/-}$ mice ($n = 3$/strain). Brain tissue was relatively hypothermic at baseline, as reported previously (Kalmbach and Waters 2012). Cortical temperature signal increased directly proportional to the light intensity, and did not differ between $ChR2^{+/-}$ and $ChR2^{-/-}$ mice (Supplemental Figure). Importantly, even at 10 mW light intensity brain temperature remained within physiological range (37.4 ± 0.5 °C).

Discussion

There is great interest in developing non-invasive experimental models in which an SD can be repeatedly and reproducibly triggered without causing any direct tissue damage. Optogenetic

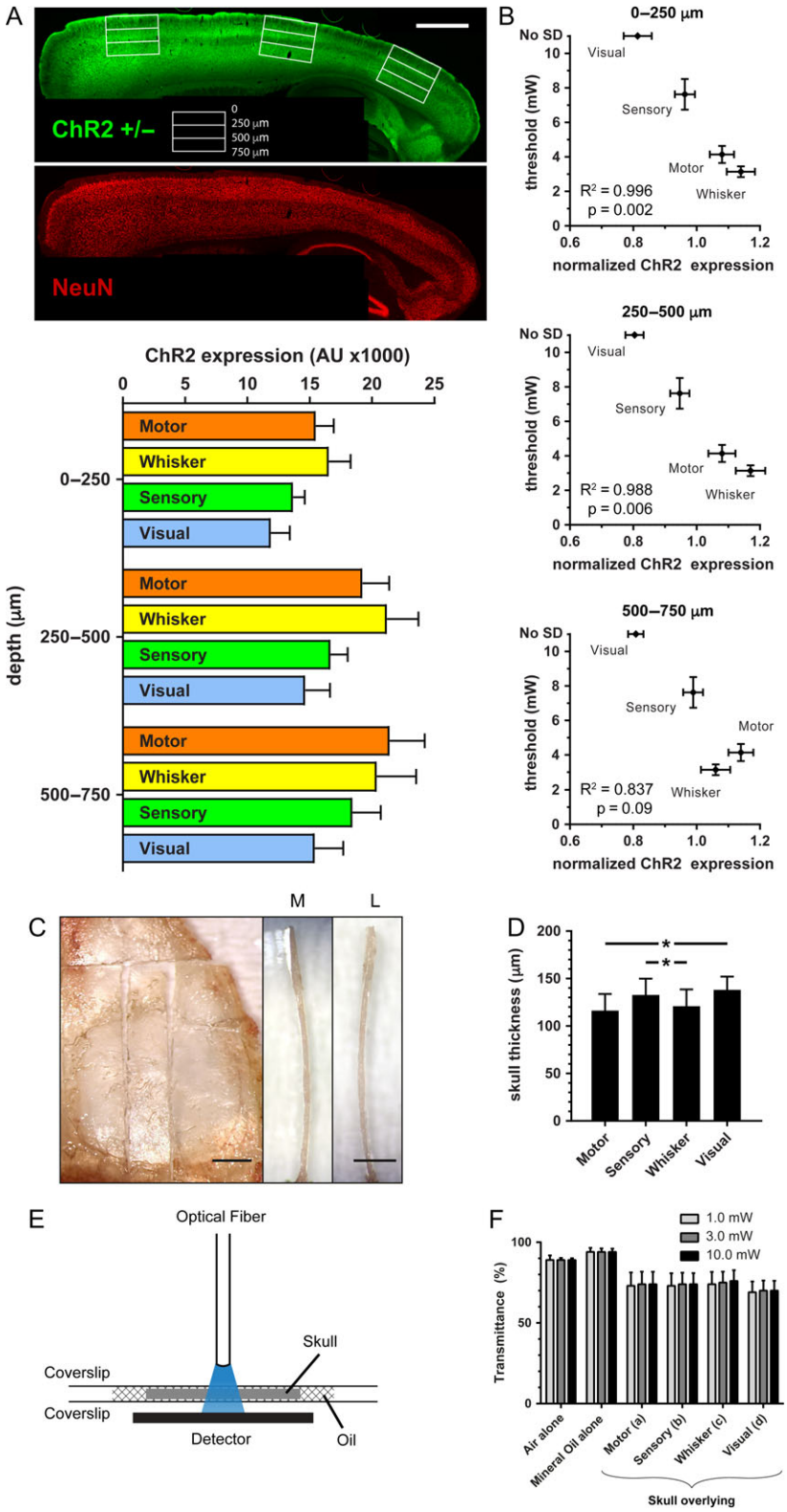

Figure 4. Channelrhodopsin-2 expression as a critical determinant of optogenetic SD threshold. (*A*) A representative sagittal section from a ChR2$^{+/-}$ mouse 2 mm lateral to midline showing ChR2 and NeuN double immunostaining. Motor, sensory, and visual cortex (from left to right) are denoted by white rectangles and cortical depth is indicated at this section level. Scale bar = 1000 μm. ChR2 fluorescence (arbitrary units, AU) in motor, whisker barrel, sensory, and visual cortices are shown at the indicated depths (n = 7 mice). (*B*) Optogenetic SD thresholds (mW) are inversely correlated (Pearson's r) with ChR2 expression (normalized to global average in AU) in the superficial but not deep layers. (*C*) Ex vivo view of the right-sided skull, sectioned so that the medial (*M*) and lateral (*L*) edges of a skull fragment overlying motor, sensory, whisker barrel, and visual cortex can be measured. Scale bar is 1 mm. (*D*) Skull thickness over motor, visual, sensory and whisker barrel cortices (*P < 0.05; 1-way repeated measures ANOVA correcting for multiple comparisons; n = 12 mice). (*E*) Schematic for light transmittance experiments. (*F*) Light transmittance did not significantly differ among different regions. Two-way ANOVA for repeated measures and correcting for multiple comparisons (n = 13 mice).

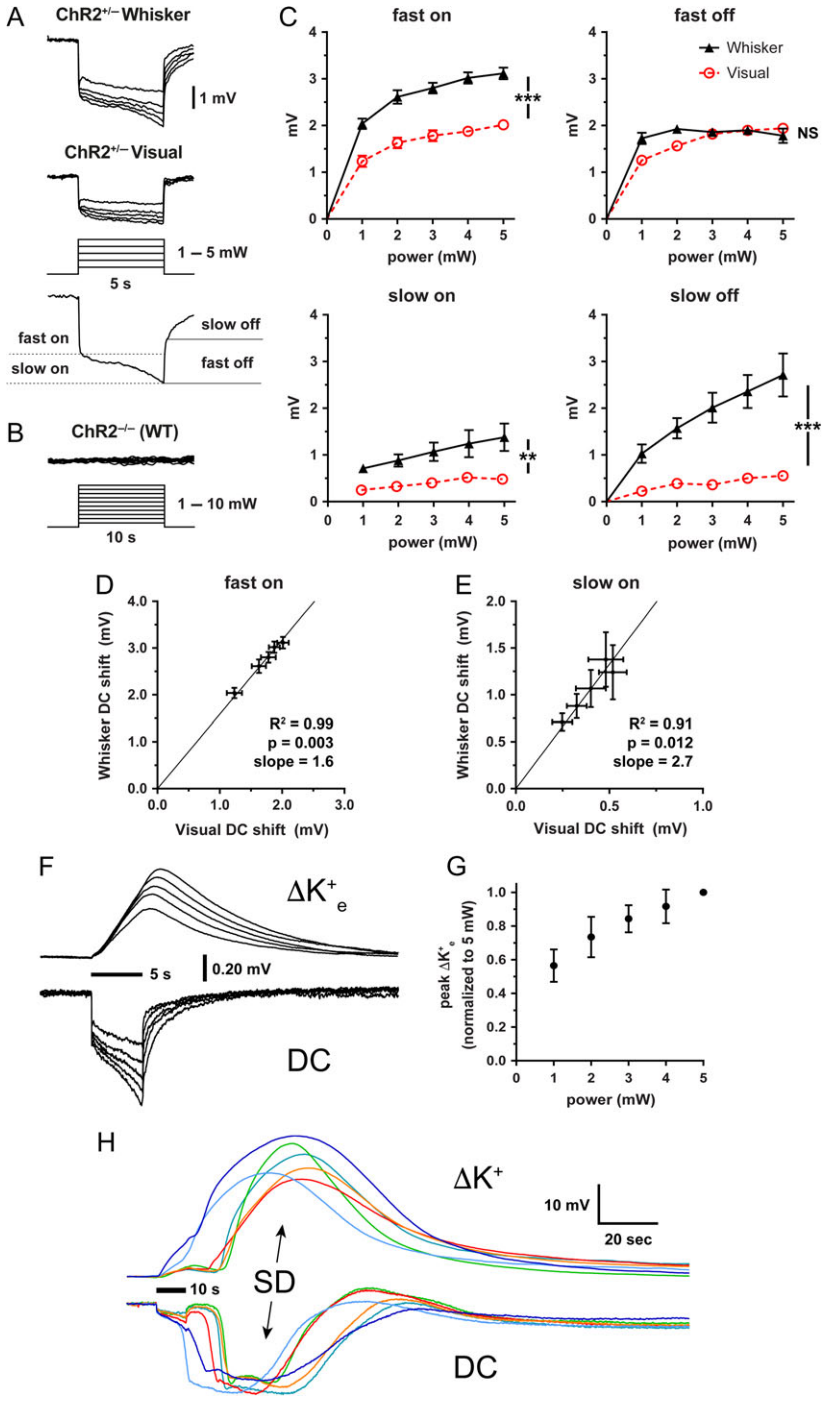

Figure 5. Extracellular potential and $[K^+]_e$ shifts during optogenetic stimulation. (*A*) Averaged extracellular potential shifts during light stimulation in whisker barrel and visual cortex at stepwise increasing light intensities (1–5 mW; $n = 9$ and 10 ChR2$^{+/-}$, respectively). The electrode tip was located directly under the light stimulation at the center of the light cone. Measurements of fast/slow on and fast/slow off potentials are indicated on a representative trace. (*B*) Representative extracellular potential recordings during light stimulation in whisker barrel cortex from a ChR2$^{-/-}$ (wild-type) mouse in response to 10-s stepwise increasing light intensities from 1–10 mW. (*C*) Extracellular potential shift power-response relationship ($n = 9$ whisker barrel cortex and 10 visual cortex in ChR2$^{+/-}$). Whisker barrel cortex consistently has significantly greater potential shifts than visual cortex except for the fast off component (***$P < 0.0001$; **$P < 0.01$; NS = not significant; 2-way ANOVA). Bars indicate ± standard error of the mean (SEM). (*D*,*E*) Slopes of the linear prediction equation represent the ratio of averaged whisker barrel vs. visual cortex fast on (*D*) and slow on (*E*) potential shifts at 1.0, 2.0, 3.0, 4.0, and 5.0 mW. Pearson's r also shown. Bars indicate ± SEM. (*F*) Optogenetic stimulation enables extracellular potassium measurements at the site of origin of SD. Averaged records showing changes in extracellular potassium-selective electrode (ΔK^+) potential shifts and direct current (DC) potential shifts from a 5-s light stimulation (horizontal bar) over whisker barrel cortex ($n = 6$ ChR2$^{+/-}$ mice). (*G*) Normalized peak extracellular potassium concentration vs. light stimulation intensity. Bars indicate ± standard deviation. (*H*) Individual extracellular potassium and concomitant DC potential tracings in response to a 10-s light stimulation (horizontal bar) that precipitates an SD. Colors correspond to specific trials ($n = 6$ ChR2$^{+/-}$ mice).

Table 2 Amplitude and duration of $[K^+]_e$ rise during SD in $ChR2^{+/-}$ and $ChR2^{-/-}$ mice

	$ChR2^{-/-}$ ($n = 6$) KCl-induced SD	$ChR2^{+/-}$ ($n = 6$) Optogenetic SD
Amplitude (mV)	28.7 ± 3.1	30.2 ± 1.8
Duration (s)	46 ± 2	52 ± 3

Data are mean ± standard deviation. $P > 0.05$, *t*-test.

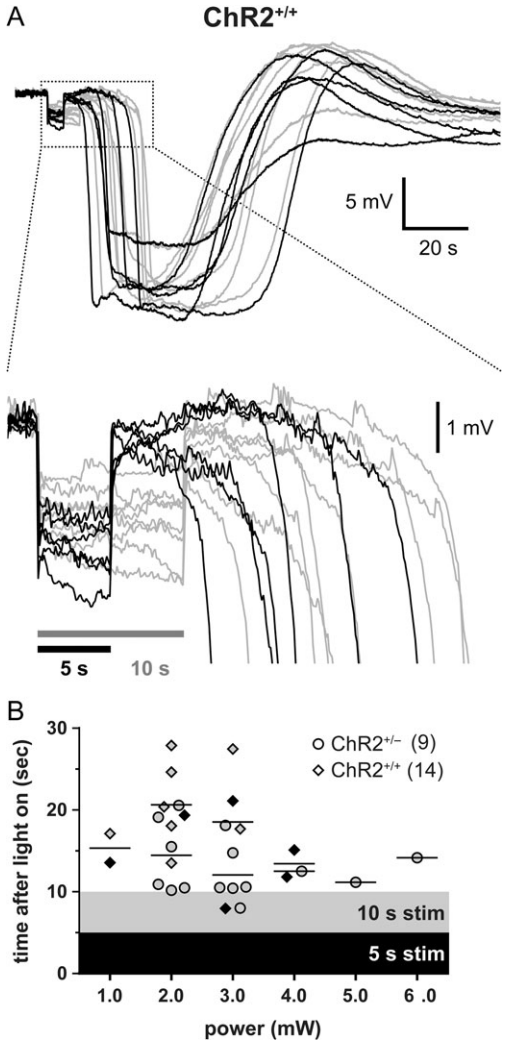

Figure 6. SD occurs with a substantial latency after light stimulation. (A) DC-potential records of individual SDs from $ChR2^{+/+}$ mice in response to either a 5- (black traces) or a 10-s (gray traces) light stimulus. Box indicates zoomed-in area. SD occurs at latencies up to 20 s after the end of light stimulation. (B) SD latencies vs. light intensity (mW) in $ChR2^{+/-}$ and $ChR2^{+/+}$ mice. Shaded areas indicate the time frame the light stimulus was applied, in order to provide a perspective on how late SDs appeared (symbols) after the end of stimulation in each strain and stimulus duration. Horizontal lines indicate mean time to an SD in $ChR2^{+/-}$ and $ChR2^{+/+}$ mice for each light intensity. Black and gray symbols represent SDs triggered by a 5- or 10-s stimulus, respectively. Sample sizes show number of mice.

excitation of cortical neurons has recently been shown capable of inducing sufficient depolarization to trigger an SD in visual cortex of $ChR2^{+/+}$ mice via an optical fiber attached to the skull (Houben et al. 2016). Building on this, we developed a practical, non-invasive and reproducible model of optogenetic SD induction and susceptibility determination that can be employed longitudinally in the same animal. We comprehensively characterized the light intensity necessary to trigger an SD, and found marked differences in susceptibility between $ChR2^{+/-}$ and $ChR2^{+/+}$ (i.e., allele-dosage), and among cortical fields, linked to the relative expression of ChR2. Moreover, we tested the modulation of optogenetic SD susceptibility by age, sex, and anesthesia duration. These are critical model features to consider in experimental design and interpretation. Importantly, using a sensitive marker of cell death we demonstrated that optogenetic SD induction does not lead to tissue damage, within the range of intensity and duration employed herein. The only other SD trigger that has been rigorously examined and shown to not cause neuronal damage has been air microembolization (Nozari et al. 2010).

The markedly lower optogenetic SD susceptibility in visual cortex was a surprising finding. Whisker barrel and primary sensory cortices have previously been suggested to be more susceptible to SD compared to motor cortex in a model of topical bath application of KCl over a wide cranial window (Bogdanov et al. 2016); however, that model did not allow direct quantitative comparisons. Therefore, to test whether innate SD susceptibility contributes to the regional differences in optogenetic thresholds, we directly quantified the electrical and KCl concentration thresholds in motor and visual cortices, representing the low and high extremes of optogenetic thresholds, respectively. Contrary to the optogenetic thresholds, we did not find higher electrical and KCl thresholds in the visual cortex. Instead, optogenetic SD susceptibility (and their corresponding local light-induced field potential amplitudes) correlated well with the relative regional ChR2 expression in the cortical fields studied.

Light-induced field potentials had distinct fast and slow components. The fast potential shifts were time-locked to light on/off cycles, and therefore, most likely a direct reflection of ChR2 currents. Interestingly, however, the amplitude of the fast component that appeared at the light onset (fast on) was always larger than the amplitude of the fast component that disappeared when the light was turned off (fast off), suggesting partial desensitization of ChR2 to light over the illumination period (Mattis et al. 2011). The slow component, on the other hand, increased progressively during the illumination superimposed on the fast component. Given the critical role of NMDA receptors in SD, and their relatively unique voltage-dependency and slow kinetics, we initially hypothesized that the slow component was mediated by NMDA receptors, but found it to be insensitive to MK-801, even at a dose that blocked all SDs (Fig. 7). The currents underlying this slow component remain enigmatic at this time.

Nevertheless, MK-801 blocked the initiation of an SD at the illumination site, and thereby unmasked a prolonged slow component of the local light-induced field potential after strong stimulation (7–10 mW for 10 s), which in some cases continued to build up into an afterpotential at the end of illumination (Fig. 7*D*). The fact that MK-801 was able to completely block the transition of local light-induced field potential to SD was inconsistent with data suggesting that NMDA receptor-mediated currents do not contribute to SD initiation (Enger et al. 2015). It should be noted, however, that most experimental models of SD cannot distinguish between inhibition of SD initiation versus propagation. By enabling simultaneous intracortical recordings from the center of illumination, optogenetic SD induction opens a window to examine the early membrane currents preceding and leading to an SD. This ability to record directly from

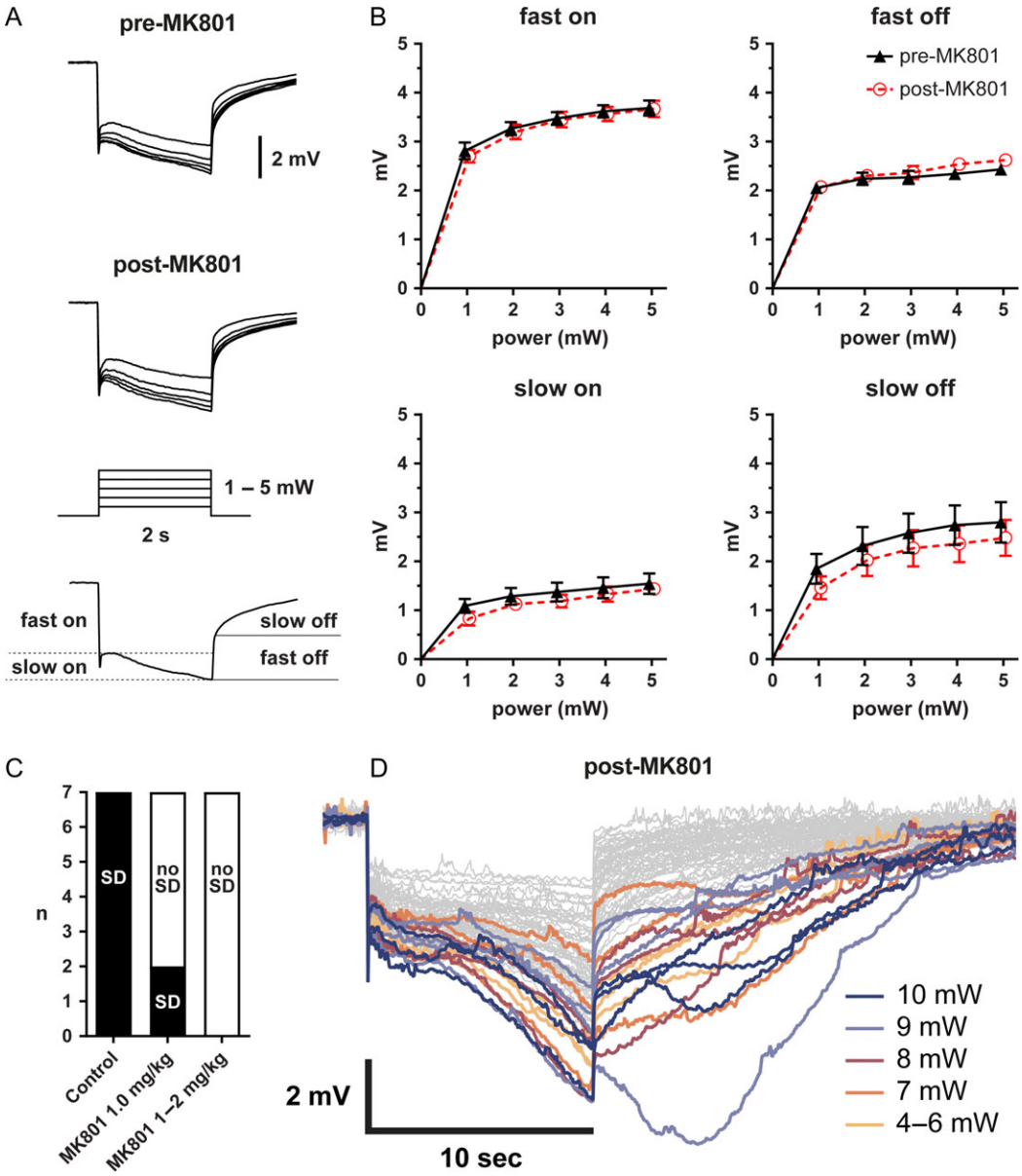

Figure 7. NMDA receptor antagonist MK-801 prevents optogenetic SD. (*A*) Averaged local field potential shifts during light stimulation in whisker barrel cortex before and after MK-801. The electrode tip was located directly under the light stimulation at the center of the light cone. (*B*) Fast and slow on and off potential shifts induced by a 2-s light stimulus pre- and post-MK-801 are not significantly different ($n = 9$ each; 2-way ANOVA). (*C*) Number of SDs induced in whisker barrel cortex using the 10-s protocol outlined in Figure 2 before and after MK-801 administration ($n = 9$ ChR2$^{+/+}$ mice pre-MK-801 and $n = 7$ post-MK-801). (*D*) Individual records in response to a 10-s light stimulus post-MK-801. Shown are 70 overlaid records from ChR2$^{+/+}$ mice. Records with a delayed afterpotential are highlighted in color.

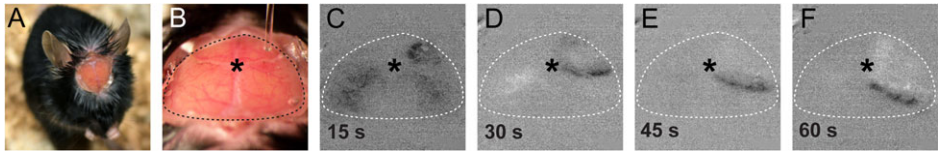

Figure 8. Chronic dosing of light-induced SD through an imaging window. (*A*) Mouse after implantation of an imaging window over intact skull. (*B*) View of the imaging window in an anesthetized mouse. An optical fiber is briefly positioned over the right frontal bone (motor cortex) for light stimulation. (*C–F*) Optical intrinsic signal difference images based on the view in *B* using a microscope objective camera showing an optogenetic SD. * = bregma.

the tissue in which SD originates revealed a markedly prolonged latency of up to 15–20 s between the end of illumination and SD onset (Fig. 6). During this post-illumination, pre-SD phase, light-induced field potentials and local $[K^+]_e$ elevations diminished (Figs 5*G* and 6), and in some cases completely returned to baseline by the time SD developed, suggesting that the cellular events triggered by exposure to light leading up to SD onset do not necessarily involve $[K^+]_e$ or membrane currents

that produce extracellular potential shifts. We also considered the possibility that SD origin was away from the recording site (i.e., not directly at the center of light cone). However, a calculation based on known SD propagation speed showed that such a distant origin must be more than 0.5 mm away from the recording electrode, which put it outside the effective penetration range of blue excitation light in cortical tissue. The possibility was further eliminated by observing the SD origin directly at the center of illumination in experiments where full-field optical imaging was employed to detect SD.

Because anesthesia suppresses innate SD susceptibility (Kudo et al. 2008), the threshold light intensities identified under isoflurane anesthesia are likely to be different from other anesthetics and unanesthetized mice. This is supported by the observation that longer anesthesia durations predicted higher thresholds in our experiments. The finding was not due to worsening systemic physiological state as arterial blood pressure, pH, pCO_2 or pO_2 remained within normal limits and did not significantly predict the threshold in multivariable analysis. In contrast to previous work in rats suggesting that SD susceptibility may decrease with age (Hablitz and Heinemann 1989; Maslarova et al. 2011; Menyhart et al. 2015), optogenetic SD susceptibility was not age-dependent within the age range in our study (12–54 weeks). Moreover, we found only a small albeit statistically significant effect of sex on optogenetic SD susceptibility, which is consistent with our prior experience in wild-type mice (Eikermann-Haerter et al. 2009).

Conclusion

We present key determinants for the non-invasive induction of SDs using optogenetics. Our model enables the study of electrophysiological events and changes in ion concentrations during stimulation and subsequent transition to SD at its origin, which are not accessible when SDs are induced by electrical, chemical, or mechanical means. This approach avoids the direct, confounding injury caused by conventional means of SD induction and will be valuable in determining the role of SDs in migraine, as well as in ischemic, hemorrhagic, or traumatic brain injury.

Supplementary Material

Supplementary material is available at *Cerebral Cortex* online.

Funding

The National Institute of Neurological Disorders and Stroke at the National Institutes of Health (P01NS055104 and R01NS102969 to C.A.; R01NS091230 and R01MH111359 to S.S.; R00AG042026 to M.A.Y.; and R25NS065743 to D.Y.C.). The National Center for Advancing Translational Sciences, National Institutes of Health Award (UL1 TR001102) to H.L. Fondation Leducq, Heitman Foundation and Ellison Foundation to C.A. Brain Aneurysm Foundation's Timothy P. Susco and Andrew David Heitman Foundation Chairs of Research to D.Y.C. International Headache Society to H.S. Japanese Heart Foundation and Bayer Yakuhin Research Grant Abroad to F.O. European Union's (EU) Seventh Framework programme "EUROHEADPAIN" (nr. 602633 to A.M.J.M. v.d.M) and EU Marie Curie IAPP Program "BRAINPATH" (nr 612360 to A.M.J.M.v.d.M and E.A.T.).

Notes

We thank Leigh Hochberg and Douglas Hayden for discussions and helpful comments. *Conflict of Interest*: None declared.

References

Anikeeva P, Andalman AS, Witten I, Warden M, Goshen I, Grosenick L, Gunaydin LA, Frank LM, Deisseroth K. 2011. Optetrode: a multichannel readout for optogenetic control in freely moving mice. Nat Neurosci. 15:163–170.

Ayata C. 2009. Spreading depression: from serendipity to targeted therapy in migraine prophylaxis. Cephalalgia. 29: 1095–1114.

Ayata C. 2010. Cortical spreading depression triggers migraine attack: pro. Headache. 50:725–730.

Ayata C. 2013. Pearls and pitfalls in experimental models of spreading depression. Cephalalgia. 33:604–613.

Ayata C, Jin H, Kudo C, Dalkara T, Moskowitz MA. 2006. Suppression of cortical spreading depression in migraine prophylaxis. Ann Neurol. 59:652–661.

Ayata C, Lauritzen M. 2015. Spreading depression, spreading depolarizations, and the cerebral vasculature. Physiol Rev. 95:953–993.

Ballanyi K, Grafe P, ten Bruggencate G. 1987. Ion activities and potassium uptake mechanisms of glial cells in guinea-pig olfactory cortex slices. J Physiol. 382:159–174.

Bogdanov VB, Middleton NA, Theriot JJ, Parker PD, Abdullah OM, Ju YS, Hartings JA, Brennan KC. 2016. Susceptibility of primary sensory cortex to spreading depolarizations. J Neurosci. 36:4733–4743.

Bosche B, Graf R, Ernestus RI, Dohmen C, Reithmeier T, Brinker G, Strong AJ, Dreier JP, Woitzik J, Members of the Cooperative Study of Brain Injury D. 2010. Recurrent spreading depolarizations after subarachnoid hemorrhage decreases oxygen availability in human cerebral cortex. Ann Neurol. 67:607–617.

Chung DY, Oka F, Ayata C. 2016. Spreading depolarizations: a therapeutic target against delayed cerebral ischemia after subarachnoid hemorrhage. J Clin Neurophysiol. 33:196–202.

Dreier JP. 2011. The role of spreading depression, spreading depolarization and spreading ischemia in neurological disease. Nat Med. 17:439–447.

Dreier JP, Major S, Manning A, Woitzik J, Drenckhahn C, Steinbrink J, Tolias C, Oliveira-Ferreira AI, Fabricius M, Hartings JA, et al, group Cs. 2009. Cortical spreading ischaemia is a novel process involved in ischaemic damage in patients with aneurysmal subarachnoid haemorrhage. Brain. 132:1866–1881.

Dreier JP, Woitzik J, Fabricius M, Bhatia R, Major S, Drenckhahn C, Lehmann TN, Sarrafzadeh A, Willumsen L, Hartings JA, et al. 2006. Delayed ischaemic neurological deficits after subarachnoid haemorrhage are associated with clusters of spreading depolarizations. Brain. 129:3224–3237.

Eikermann-Haerter K, Can A, Ayata C. 2012. Pharmacological targeting of spreading depression in migraine. Expert Rev Neurother. 12:297–306.

Eikermann-Haerter K, Dilekoz E, Kudo C, Savitz SI, Waeber C, Baum MJ, Ferrari MD, van den Maagdenberg AM, Moskowitz MA, Ayata C. 2009. Genetic and hormonal factors modulate spreading depression and transient hemiparesis in mouse models of familial hemiplegic migraine type 1. J Clin Invest. 119:99–109.

Eikermann-Haerter K, Lee JH, Yalcin N, Yu ES, Daneshmand A, Wei Y, Zheng Y, Can A, Sengul B, Ferrari MD, et al. 2015.

Migraine prophylaxis, ischemic depolarizations, and stroke outcomes in mice. Stroke. 46:229–236.

Eikermann-Haerter K, Yuzawa I, Dilekoz E, Joutel A, Moskowitz MA, Ayata C. 2011. Cerebral autosomal dominant arteriopathy with subcortical infarcts and leukoencephalopathy syndrome mutations increase susceptibility to spreading depression. Ann Neurol. 69:413–418.

Enger R, Tang W, Vindedal GF, Jensen V, Johannes Helm P, Sprengel R, Looger LL, Nagelhus EA. 2015. Dynamics of ionic shifts in cortical spreading depression. Cereb Cortex. 25: 4469–4476.

Fabricius M, Fuhr S, Willumsen L, Dreier JP, Bhatia R, Boutelle MG, Hartings JA, Bullock R, Strong AJ, Lauritzen M. 2008. Association of seizures with cortical spreading depression and peri-infarct depolarisations in the acutely injured human brain. Clin Neurophysiol. 119:1973–1984.

Hablitz JJ, Heinemann U. 1989. Alterations in the microenvironment during spreading depression associated with epileptiform activity in the immature neocortex. Brain Res Dev Brain Res. 46:243–252.

Hartings JA, Shuttleworth CW, Kirov SA, Ayata C, Hinzman JM, Foreman B, Andrew RD, Boutelle MG, Brennan KC, Carlson AP, et al. 2016. The continuum of spreading depolarizations in acute cortical lesion development: Examining Leao's legacy. J Cereb Blood Flow Metab. 37:1571–1594.

Houben T, Loonen IC, Baca SM, Schenke M, Meijer JH, Ferrari MD, Terwindt GM, Voskuyl RA, Charles A, van den Maagdenberg AM, et al. 2016. Optogenetic induction of cortical spreading depression in anesthetized and freely behaving mice. J Cereb Blood Flow Metab. 37:1641–1655.

Kalmbach AS, Waters J. 2012. Brain surface temperature under a craniotomy. J Neurophysiol. 108:3138–3146.

Kudo C, Nozari A, Moskowitz MA, Ayata C. 2008. The impact of anesthetics and hyperoxia on cortical spreading depression. Exp Neurol. 212:201–206.

Leão A. 1944. Spreading depression of activity in the cerebral cortex. J Neurophysiol. 7:359–390.

Maslarova A, Alam M, Reiffurth C, Lapilover E, Gorji A, Dreier JP. 2011. Chronically epileptic human and rat neocortex display a similar resistance against spreading depolarization in vitro. Stroke. 42:2917–2922.

Mattis J, Tye KM, Ferenczi EA, Ramakrishnan C, O'Shea DJ, Prakash R, Gunaydin LA, Hyun M, Fenno LE, Gradinaru V, et al. 2011. Principles for applying optogenetic tools derived from direct comparative analysis of microbial opsins. Nat Methods. 9:159–172.

Menyhart A, Makra P, Szepes BE, Toth OM, Hertelendy P, Bari F, Farkas E. 2015. High incidence of adverse cerebral blood flow responses to spreading depolarization in the aged ischemic rat brain. Neurobiol Aging. 36:3269–3277.

Nozari A, Dilekoz E, Sukhotinsky I, Stein T, Eikermann-Haerter K, Liu C, Wang Y, Frosch MP, Waeber C, Ayata C, et al. 2010. Microemboli may link spreading depression migraine aura and patent foramen ovale. Ann Neurol. 67:221–229.

Oka F, Hoffmann U, Lee JH, Shin HK, Chung DY, Yuzawa I, Chen SP, Atalay YB, Nozari A, Hopson KP, et al. 2016. Requisite ischemia for spreading depolarization occurrence after subarachnoid hemorrhage in rodents. J Cereb Blood Flow Metab. 37:1829–1840.

Paxinos G, Franklin KBJ. 2001. The mouse brain in stereotaxic coordinates. San Diego: Academic Press.

Silasi G, Xiao D, Vanni MP, Chen AC, Murphy TH. 2016. Intact skull chronic windows for mesoscopic wide-field imaging in awake mice. J Neurosci Methods. 267:141–149.

Uhlirova H, Kilic K, Tian P, Thunemann M, Desjardins M, Saisan PA, Sakadzic S, Ness TV, Mateo C, Cheng Q, et al. 2016. Cell type specificity of neurovascular coupling in cerebral cortex. Elife. 5:e14315.

von Bornstadt D, Houben T, Seidel JL, Zheng Y, Dilekoz E, Qin T, Sandow N, Kura S, Eikermann-Haerter K, Endres M, et al. 2015. Supply-demand mismatch transients in susceptible peri-infarct hot zones explain the origins of spreading injury depolarizations. Neuron. 85:1117–1131.

Wang H, Peca J, Matsuzaki M, Matsuzaki K, Noguchi J, Qiu L, Wang D, Zhang F, Boyden E, Deisseroth K, et al. 2007. High-speed mapping of synaptic connectivity using photostimulation in Channelrhodopsin-2 transgenic mice. Proc Nat Acad Sci USA. 104:8143–8148.